Theor Appl Climatol (2013) 113:95–103
DOI 10.1007/s00704-012-0767-y

ORIGINAL PAPER

Impact of 3-D topography on surface radiation budget over the Tibetan Plateau

Wei-Liang Lee · K. N. Liou · Chia-chi Wang

Received: 9 May 2012 / Accepted: 9 September 2012 / Published online: 29 September 2012

Abstract The 3-D complex topography effect on the surface solar radiative budget over the Tibetan Plateau is investigated by means of a parameterization approach on the basis of "exact" 3-D Monte Carlo photon tracing simulations, which use 90 m topography data as building blocks. Using a demonstrative grid size of 10×10 km^2, we show that differences in downward surface solar fluxes for a clear sky without aerosols between the 3-D model and the conventional plane-parallel radiative transfer scheme are substantial, on the order of 200 W/m^2 at shaded or sunward slopes. Deviations in the reflected fluxes of the direct solar beam amount to about +100 W/m^2 over snow-covered areas, which would lead to an enhanced snowmelt if the 3-D topography effects had been accounted for in current climate models. We further demonstrate that the entire Tibetan Plateau would receive more solar flux by about 14 W/m^2, if its 3-D mountain structure was included in the calculations, which would result in larger sensible and latent heat transfer from the surface to the atmosphere.

W.-L. Lee (✉)
Research Center for Environmental Changes, Academia Sinica,
128 Academia Rd. Sec. 2,
Taipei, Taiwan
e-mail: leelupin@gate.sinica.edu.tw

K. N. Liou
Joint Institute for Regional Earth System Science and Engineering
and Department of Atmospheric and Oceanic Sciences,
University of California, Los Angeles,
405 Hilgard Ave,
Los Angeles, CA 90095, USA

C.-c. Wang
Department of Atmospheric Sciences, Chinese Culture University,
55 Hwa-Kang Rd.,
Taipei, Taiwan

1 Introduction

Surface solar fluxes over complex mountain structure are significantly modulated by variation in terrain elevation, slope, and aspect (see, e.g., Dubayah et al. 1990; Dubayah and Rich 1995). Because of the complexity of spatial orientation and the optical properties of the surface, however, these factors have not been accounted for in the contemporary radiative transfer schemes that have been used in weather and climate models. In these models, the lower boundary is assumed to be unobstructed, horizontal, and homogeneous.

Using topographic information, several approaches with varying degrees of sophistication have been developed to evaluate solar fluxes at the surface (e.g., Dozier and Frew 1990; Dubayah et al. 1990; Essery and Marks 2007; Lai et al. 2010). However, the anisotropic nature of the diffuse flux and multiple reflection over complex topography have not been accounted for in these approaches, as illustrated in the papers by Dubayah and Rich (1995) and Wang et al. (2005). Additionally, the topography effect can lead to substantial uncertainty in the estimation of downward solar radiation using satellite remote sensing data (Yang et al. 2008). For these reasons, a more accurate approach is required.

Intricate interactions between the solar beam and irregular lower boundaries such as wind-blown sea surfaces and canopies have been investigated by means of 3-D Monte Carlo approaches (e.g., Preseindorfer and Mobley 1986; Govaerts and Verstraete 1998; Lee and Liou 2007; Iwabuchi and Kobayashi 2008; Mayer et al 2010). Chen et al. (2006) developed a 3-D Monte Carlo radiative transfer model to "exactly" calculate solar fluxes over rugged surfaces in clear sky conditions. Liou et al. (2007) followed this 3-D model to compute the surface fluxes over a 100×100-km^2 area in the Tibetan Plateau and showed that the domain-average solar surface flux over a regional model scale (e.g., 50×

50 km^2) consisting of intense topography can deviate from the flux over a smoothed surface by 10–50 W/m^2. Further to this work, Lee et al. (2011) (hereafter LLH) improved this Monte Carlo approach using a new land surface configuration consisting of more realistic 3-D triangles, replacing stair-like rectangles that were used in previous analysis.

The 3-D Monte Carlo photon tracing program is the most physically "exact" approach for calculating radiative transfer involving mountains, but this approach is computationally expensive and therefore its direct implementation in climate models seems impractical. To account for the effects of shadowing and multiple reflection on clear sky solar fluxes received by mountainous surfaces, LLH developed a parameterization approach based on simulations from the 3-D Monte Carlo photon tracing program. Through multiple linear regression, this parameterization utilizes topographic information such as elevation, sky view factor, and terrain configuration factor, as independent variables. By using the digital elevation model (DEM) at a resolution of 1 km, LLH found that the regression equations can on average explain over 90 % of the variation in the direct, direct-reflected, and diffuse-reflected fluxes, which include values larger than 100 W/m^2.

This study follows the parameterization approach developed by LLH to evaluate the broadband solar fluxes over Earth's most intense terrain, the Tibetan Plateau, and investigates the 3-D topography effect on surface radiative energy budget. In Section 2, we describe an improved parameterization approach that utilizes the topography data with a 90-m resolution, which is applied to the Tibetan Plateau in order to analyze the deviation of surface radiative fluxes in mountains from unobstructed horizontal surfaces (Section 3). In Section 4, we investigate the temporal and spatial variability in the 3-D topography effect and discuss its possible impact on climate modeling. Conclusions are given in Section 5.

2 Parameterization for surface solar flux calculation

The sunlight or solar fluxes that reach the surface can be physically grouped into the following five components: (1) The direct flux (F_{dir}) is composed of photons from the sun directly striking the surface without experiencing scattering or reflection. (2) The diffuse flux (F_{dif}) is associated with photons undergoing single and/or multiple scattering by air molecules without surface reflection. (3) The direct-reflected flux (F_{rdir}) consists of photons directly from the sun without encountering scattering but which are subsequently reflected by surrounding terrain. (4) The diffuse-reflected flux (F_{rdif}) resembles the direct-reflected flux defined in (3), except that the photons are first scattered by air molecules and afterwards reflected by nearby terrain. (5) The coupled flux (F_{coup}) is defined by photons which encounter surface reflection or atmospheric scattering after being reflected by the ground.

Both F_{dir} and F_{dif}, the direct and diffuse fluxes, are independent of surface albedo. The flux components, F_{rdir} and F_{rdif}, however, are proportional to surface albedo, since they include photons that have been reflected once. The final flux term, F_{coup}, has a nonlinear relationship with surface albedo because some of the photons in this category encounter multiple reflection. It should be noted that the diffuse flux, F_{dif}, described in this parameterization is different from that defined in conventional radiative transfer schemes, where it is the summation of F_{dif} and F_{coup}.

Existing climate models use conventional plane-parallel radiative transfer schemes to calculate solar fluxes in relation to a flat surface defined by a given elevation. Therefore, the object of LLH's parameterization was to determine the relative deviations of the five flux components from the surface fluxes corresponding to an unobstructed horizontal surface at the same mean elevation available from a climate model. Using this method, the derived deviations can be used directly in any climate models to account for the effect of topography on solar flux distribution.

As an experimental test bed, LLH randomly chose 80 10×10 km^2 rugged domains in the Sierra Nevada area using the 1-km resolution DEM data. Dubayah et al. [1989] demonstrated in their study that the distribution of surface solar fluxes over mountains is sensitive to spatial resolution and determined that substantial flux errors could be produced with grid cells larger than 200 m. To improve parameterization accuracy, we have adopted the Shuttle Radar Topography Mission (SRTM) topography data at a resolution of 90 m (Jarvis et al. 2008) to perform 3-D Monte Carlo simulations for domains corresponding to those used by LLH. To optimize the calculations, seven different solar zenith angles (SZA) were chosen (cosine of SZA, $\cos\theta_0$, of 0.1, 0.25, 0.4, 0.55, 0.7, 0.85, and 1.0). Results with SZAs in between these angles are determined by linear interpolation.

We first introduce the concept of the solar incident angle (μ_i), sky view factor (V_d), and terrain configuration factor (C_t) to prepare the independent variables for regression. On an unobstructed slope, the direct flux from the sun is related to the cosine of the solar incident angle, defined as the angle between the direction of a solar beam and the normal vector of an inclined surface. While the solar incident angle varies with time, its mean value can be obtained with a lookup table of several derivative variables related to the slope and aspect of the surface. The portion of the sky dome visible to the target point is defined as the sky view factor, and the area of surrounding mountains visible to the target point (Dozier and Frew 1990) is defined as the terrain configuration factor. The values of both variables are in the range

from 0 to 1. These two variables are widely used in estimating the diffuse and reflected fluxes over rugged surfaces. To improve the regression parameterization, we have defined the following normalized variables in the forms

$$\widetilde{\mu}_i = \frac{\mu_i}{\cos\theta_s},\ \widetilde{V}_d = \frac{V_d}{\cos\theta_s},\ and\ \widetilde{C}_t = \frac{C_t}{\cos\theta_s} \tag{1}$$

where θ_s is the slope angle of the surface.

For each 10×10-km^2 domain, conventional topographic parameters such as mean elevation and slope, along with their standard deviation and skewness, are also included as independent variables for multiple linear regression. However, several independent variables are highly correlated to one another, so some must be eliminated. Consequently, we have removed one of the variables when the correlation between two of them is greater than 0.9. Further, if the regression coefficient of an independent variable differs insignificantly from 0 based on the t test at the 90 % confidence level, this variable is removed from the regression equation.

Following LLH's approach, the flux deviation in each component for a clear sky without aerosols can be expressed by

$$\begin{pmatrix} F'_{\mathrm{dir}} \\ F'_{\mathrm{dif}} \\ F'_{\mathrm{rdir}} \\ F'_{\mathrm{rdif}} \\ F'_{\mathrm{coup}} \end{pmatrix} = \begin{pmatrix} a_1 \\ a_2 \\ a_3 \\ a_4 \\ a_5 \end{pmatrix} + \begin{pmatrix} b_{11} & b_{12} & 0 & 0 \\ b_{21} & b_{22} & 0 & b_{24} \\ 0 & b_{32} & b_{33} & 0 \\ 0 & b_{42} & b_{43} & 0 \\ b_{51} & b_{52} & b_{53} & 0 \end{pmatrix} \begin{pmatrix} \langle\widetilde{\mu}_i\rangle \\ \langle\widetilde{V}_d\rangle \\ \langle\widetilde{C}_t\rangle \\ \sigma(h) \end{pmatrix} \tag{2}$$

where $\sigma(h)$ is the standard deviation of elevation h, F'_i is the relative deviation of each flux component, a_i is the interception, b_{ij} is the regression coefficient for a specific independent variable, and angle brackets denote the spatial mean of the variable within a 10×10-km^2 domain. It is noted that all skewness and all but one standard deviation are eliminated from the regression equations. Since F'_{coup} is not a linear function of surface albedo, we have used four uniform albedo values of 0.1, 0.3, 0.5, and 0.7 in 3-D Monte Carlo simulations to account for albedo variation in regression coefficients. In Fig. 1, we compare the deviations in five flux components at an SZA of 57° between the "exact" values from 3-D Monte Carlo simulations and the values predicted by regression equations and also illustrate the coefficients of determination (R^2) as a function of $\cos\theta_0$. The values of R^2 for $F'_{\mathrm{dir}}, F'_{\mathrm{rdir}}$, and F'_{rdif} are close to unity, except when the sun is very low. The explanatory powers of the regression equations for F'_{dif} and F'_{coup} are less than those for other three components. In general, the performance of the new parameterization is better than that in LLH for all components.

It is noted that the variables employed in the new regression equations slightly differ from those obtained by LLH using the topography data at a 1-km resolution. For example, $\widetilde{V}_d$ and $\widetilde{C}_t$ are both used for the reflected fluxes. While the correlation between V_d and C_t is very close to −1, as shown by LLH, the correlation between $\widetilde{V}_d$ and $\widetilde{C}_t$ is only −0.67 so that both can be used as input variables for the reflected-related fluxes. In the parameterizations developed by previous studies (e.g., Dozier and Frew 1990; Dubayah et al. 1990), the reflected radiation received by a target is simply proportional to C_t, the surrounding mountain areas visible by the target. However, some of these areas may have already been shaded and reflect very little or no radiation to the target. The advantage of the new regression equations is that the inclusion of both $\widetilde{V}_d$ and $\widetilde{C}_t$ can account for this effect, particularly for high-resolution topography data.

3 Surface solar fluxes over the Tibetan Plateau

The mighty Tibetan Plateau, with an area of about 2.4 million km^2 and an average height of 4.7 km, profoundly influences the general circulation of the atmosphere because of its uplift of large-scale flows and its insertion of heating with a confining lower boundary at high levels. The elevated heat source in the summer has been broadly recognized in conjunction with the Indian and East Asian summer monsoons (Molnar et al. 1993; Qiu 2008). What remains largely unresolved, however, are problems related to the vertical profile of shortwave radiative heating rates over the mountainous region and the snow-albedo feedback associated with regional and global climate change. In the following, we present a number of pertinent results over the Tibetan Plateau to establish the importance of terrain inhomogeneity and irregularity to surface fluxes which in turn are crucial for the understanding of land–atmosphere interactions, boundary layer processes, and atmospheric heating/cooling rates and circulations.

A region of 25°N–40°N and 70°E–110°E was selected to cover the Tibetan Plateau. Topography with a 90-m resolution taken from the SRTM data was interpolated into 180×336 cells with a grid size of 10×10 km^2. Subsequently, the spatial means of elevation, sky view factor, and terrain factor for each domain, as well as their standard deviations, can be calculated to build a lookup table. The input parameters for 3-D radiative transfer calculations include temperature and water vapor profiles from the European Centre for Medium-Range Weather Forecasts (ECMWF) reanalysis data at a 1° resolution and broadband surface albedo for the entire solar spectrum from the Moderate Resolution Imaging Spectroradiometer (MODIS) remote sensing data at a 0.05° resolution. Since valley elevations are on average

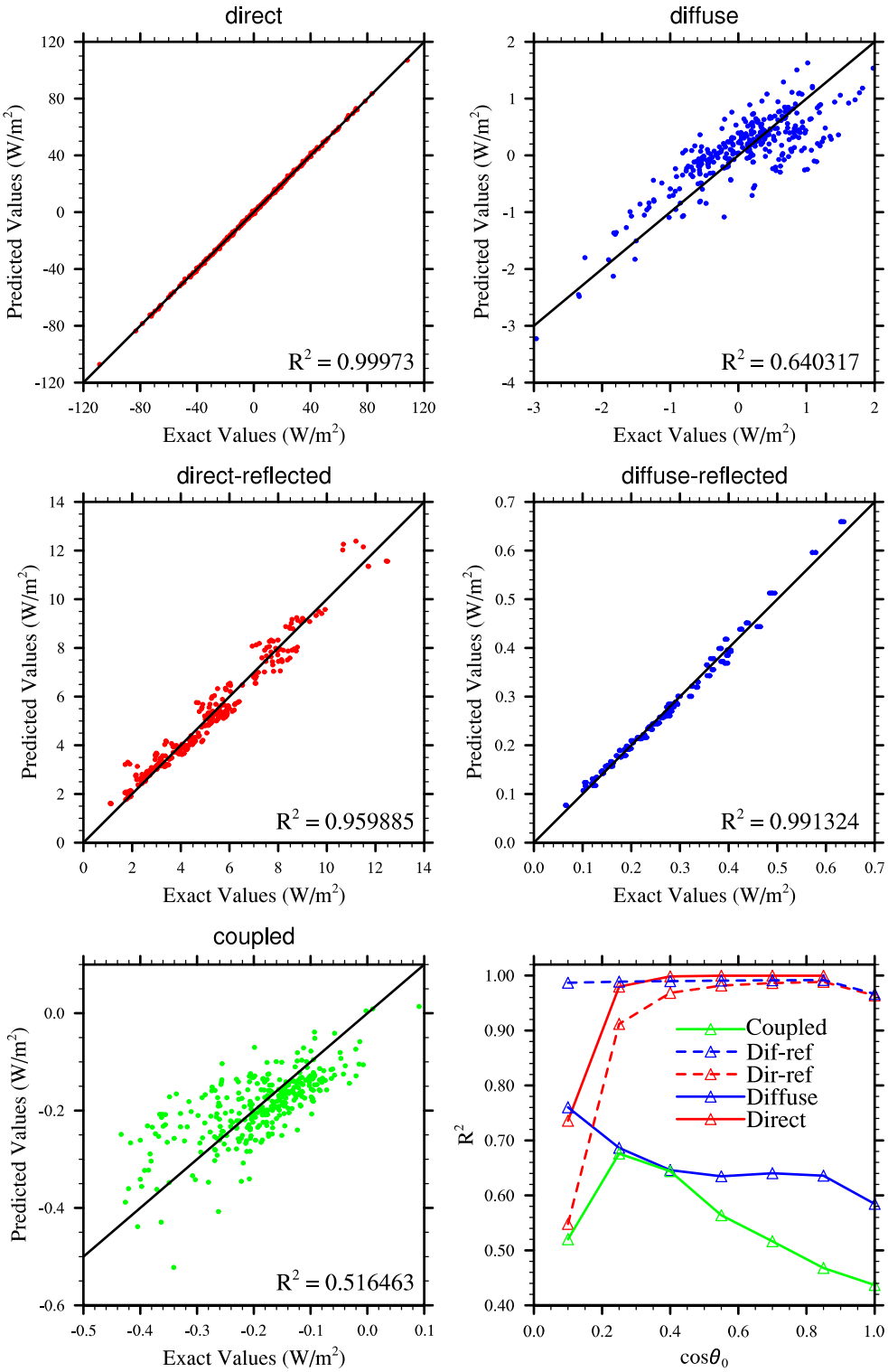

Fig. 1 Comparison between the results from the 3-D Monte Carlo simulation (exact values) and the multiple linear regression analysis (predicted values) for all flux components at an SZA of 57°. Also shown is the coefficient of determination (R^2) as a function of the cosine of SZA (*lowest panel on the right*)

lower than the bottom levels in reanalysis data, we have extrapolated the vertical profiles to mountainous surfaces. Calculations also utilized the ozone and other trace gaseous profiles for the standard midlatitude atmosphere. Figure 2 shows the elevation maps and the monthly mean of surface albedo for March 2001 over the Tibetan Plateau at a 10-km resolution. High-albedo areas, generally associated with snow cover, are located near the Pamir and Karakoram mountains.

The 1-D plane-parallel radiative transfer scheme developed by Fu and Liou (1992) and further improved by Gu et al. (2003, 2006) was employed to calculate clear sky surface solar fluxes on flat surfaces. Figure 3a shows the total

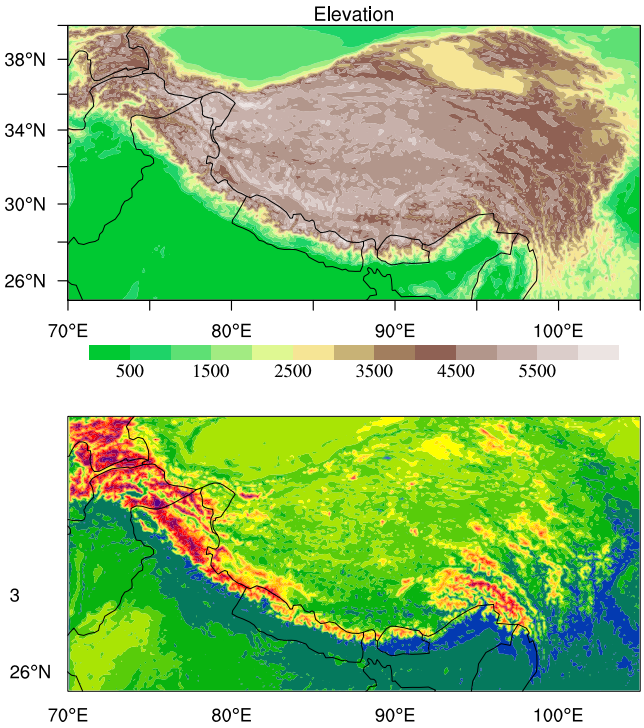

Fig. 2 Maps of the elevation (unit in meter) and monthly mean albedo for March 2001 in the Tibetan Plateau

downward flux over the Tibetan Plateau for the case of 21 March 2001 (spring equinox), at noon. Due to less atmospheric attenuation, high-elevation areas over the Himalayas receive greater solar radiation. Smaller downward fluxes are also present in high-latitude areas associated with larger solar zenith angles.

Using plane-parallel fluxes and the topography data as input variables following the parameterization approach, deviations in the five flux components can be determined. Figure 3b depicts positive F'_{dir}, the deviation in direct fluxes, at the southern face of the mountains, where the solar incident angle on the inclined surface is smaller than that on a horizontal surface, resulting in greater solar energy interception. Negative F'_{dir} occurs at the northern face of the mountains and deep valleys, where the solar beam is shaded by the slope and blocked by surrounding mountains, respectively. As shown in Fig. 3b, negative and positive deviations in direct fluxes respectively reach −200 and 200 W/m^2.

In Fig. 3c, deviations in the diffuse fluxes, F'_{dif}, range from −10 to 5 W/m^2, much smaller than F'_{dir}. In general, the values of F'_{dif} are negative in mountainous regions since the sky view factors are less than 1 in valleys. Since the phase function maxima for Rayleigh scattering reside at the forward and backward directions for the unpolarized light beam, the majority of scattered photons move in the same direction as the direct solar beam, resulting in positive F'_{dif} at some of the southern sides of the mountains.

Figure 3d shows deviations in the direct-reflected fluxes F'_{rdir}, which value is always positive because the direct-reflected- and diffuse-reflected fluxes do not exist over unobstructed horizontal surfaces. Over the intense mountainous areas with high albedo, the values of F'_{rdir} can be as large as 200 W/m^2. The spatial distribution of the diffuse-reflected fluxes F'_{rdif} is about the same as that of F'_{rdir}, as shown in Fig. 3e, except that the magnitude is much smaller with a maximum value of only about 6 W/m^2.

Figure 3f is a map of the deviations in coupled fluxes F'_{coup}, which contains two components: Photons which are reflected by the surface and subsequently backscattered by the atmosphere to the target and photons which encounter multiple surface reflection. When albedo is larger than about 0.3, the multiple reflection effect dominates. It follows that F'_{coup} increases with terrain configuration factor. Large F'_{coup} values occur at high-albedo areas with a maximum value of about 40 W/m^2. Over a less reflective surface, the first component is more important so that F'_{coup} is primarily controlled by the sky view factor. Therefore, F'_{coup} is generally negative over low-albedo areas because the sky view factor of these areas must be equal to or less than that over unobstructed horizontal surfaces. Thus, these areas receive reduced backscattered radiation from the atmosphere, which results in negative deviations.

4 Implications of the 3-D topography effect on surface solar radiation

4.1 Diurnal variations in domain-averaged downward fluxes

Figure 4a depicts the diurnal variation in deviations in the domain-averaged downward radiation for the entire Tibetan Plateau at the spring equinox. At noon, the total flux deviates from its flat surface counterpart by about 14 W/m^2. F'_{rdir} is the dominant component, contributing to about 13 W/m^2, while the averages of deviations in other flux components are close to 0. In the early morning and late afternoon, F'_{dir} is negative due to the shading effect of mountains near domain boundaries. At other times, F'_{dir} is close to 0 because its variation is evened out by the compensation effect of various orientations of slopes over a large domain. Although F'_{coup} is quite large over certain reflective areas, its spatial mean over the entire region is averaged out by smaller negative values over less rugged and low-albedo areas and is also close to 0.

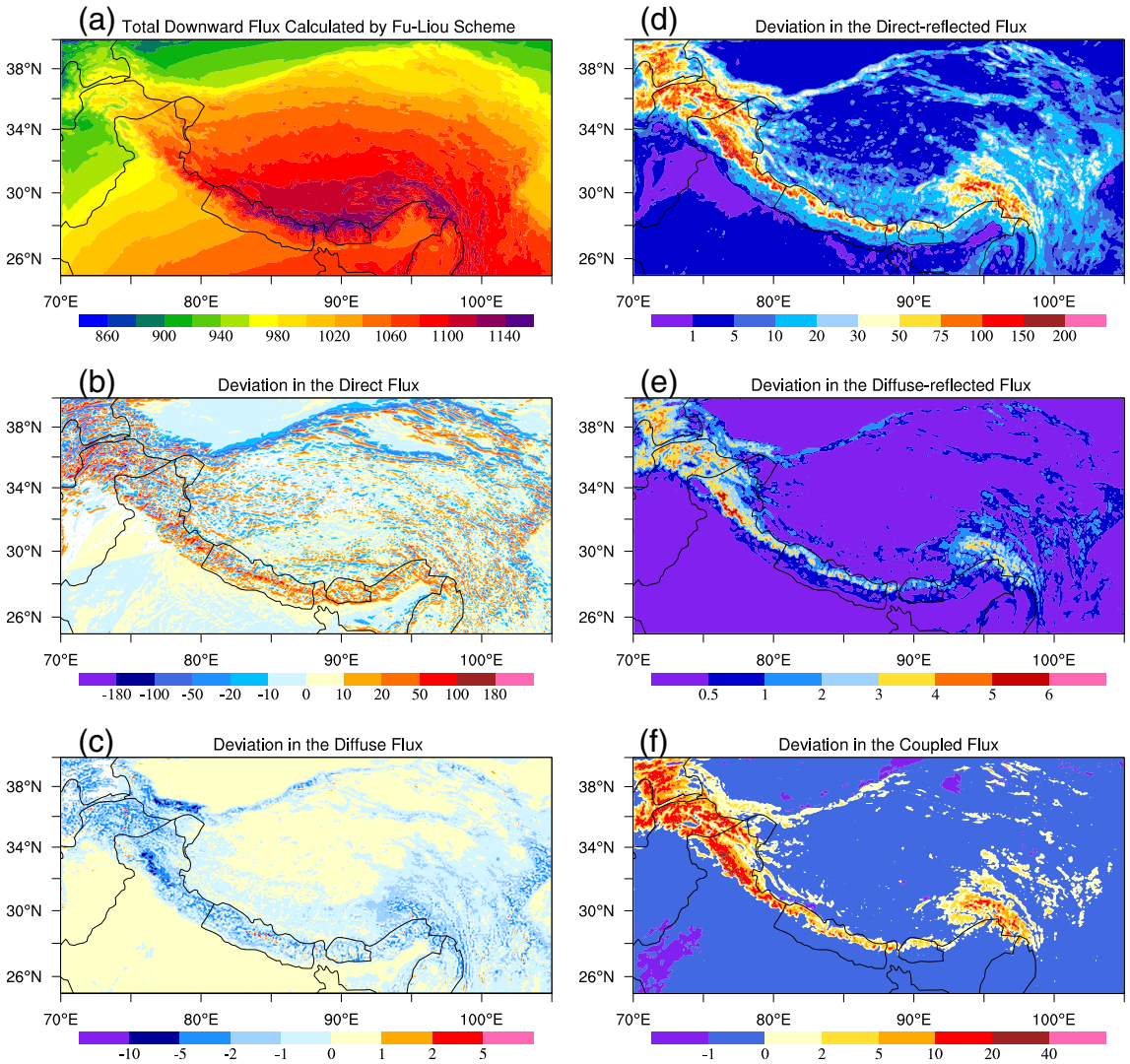

Fig. 3 **a** Total downward surface solar flux for noon, 21 March 2001, calculated by the plane-parallel Fu–Liou radiative transfer scheme; **b** deviations in the direct flux; **c** deviations in the diffuse flux; **d** deviations in the direct-reflected flux; **e** deviations in the diffuse-reflected flux; and **f** deviations in the coupled flux. **b**–**f** Reference to 3-D results

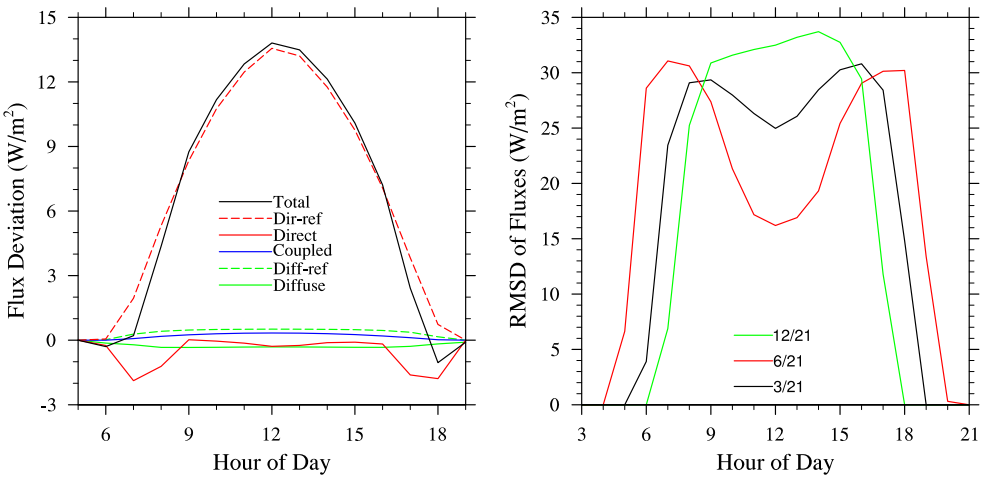

Fig. 4 Diurnal variations in the domain-averaged total downward flux and five flux components for 21 March 2001 (*left panel*), and RMSD for 21 March, 21 June, and 21 December (*right panel*)

Figure 4b shows the diurnal variation in surface fluxes between the results calculated from the 3-D model and its plane-parallel counterpart for spring equinox (March 21), summer solstice (June 21), and winter solstice (December 21) in terms of root mean square deviation (RMSD). Comparing the magnitude of deviations for each component shown in Fig. 3, the majority of RMSD is caused by F'_{dir}. During the winter solstice, a maximum value of about 34 W/m^2 is reached near noon, associated with the time of greatest incoming solar energy. However, for summer solstice, RMSD is much smaller at noon than early morning and late afternoon because the sun is near its zenith, during which the shading effect is small. At spring equinox, the diurnal variation curve falls between the two. The autumn equinox result is about equal to spring equinox, though the values are smaller due to lower albedo in September.

4.2 Sensitivity of the topography effect to spatial resolutions

This study's parameterization is developed for a 10×10-km^2 area, representative of a grid size of traditional weather models. As demonstrated in the previous section, considerable flux deviations on the order of 200 W/m^2 could be produced at this scale over the Tibetan Plateau. However, the topography effect on surface solar fluxes decreases as the spatial resolution becomes coarser. In a larger grid cell, the mountains and valleys in the subgrid scale are evened out so that the slope of the surface becomes smaller, leading to a decrease shading effect. In order to investigate the significance of the topography effect at a coarser resolution, all necessary topographic variables within 30×30 and 100×100 km^2 domains are utilized as inputs to the current regression equations for flux calculations.

In Fig. 5, deviation in the total net surface solar flux is shown for all five components at grid sizes of 10×10, 30×30, and 100×100 km^2. The deviation value for the 10-km resolution ranges from −150 to 180 W/m^2. Positive deviations occur at the southern side of the mountains and high-albedo areas, due primarily to smaller solar incident angles and stronger reflected radiation. Negative deviations are generally located at the northern side of the mountains and deep valleys, which are blocked by surrounding mountains and/or shaded by the slope. Deviation for the 30-km resolution is smaller, at a range of −42 to 90 W/m^2. Compared to the 10-km resolution, the majority of the fine structure of positive–negative pairs at the northern–southern side of mountains disappears due to smoother topography. Negative deviations are located only at very extensive and broad ridgelines such as the Kunlun Mountains; however, strong positive deviations at high-albedo areas remain. The spatial mean of C_t was obtained by taking C_t for each 90×90 m^2 pixels within a 10×10-km^2 (or 30×30 km^2) grid cell; as a result, more valleys in a grid cell lead to a greater mean C_t

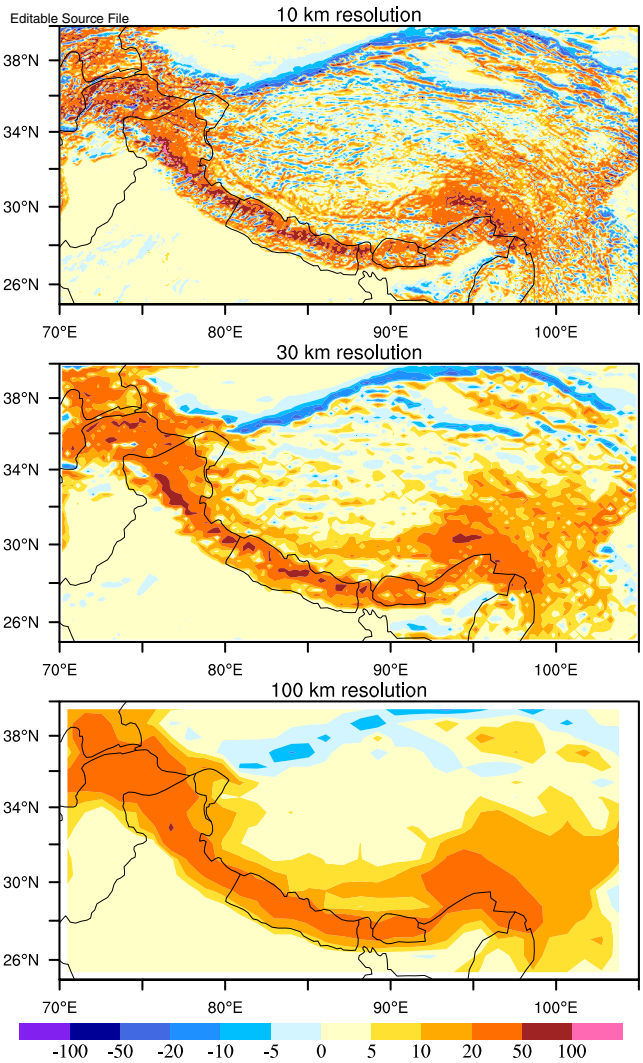

Fig. 5 Maps of the deviation in the net surface flux for noon, 21 March 2001, at resolutions of 10, 30, and 100 km

value. The 90×90-m^2 data were used in the parameterization calculations to obtain the parameter C_t. Due to this reason, substantial variability in the reflect-related fluxes remains over a large domain. Even at a 100-km resolution, strong positive deviations can be found on the order of 20 W/m^2, a value that cannot be overlooked in energy budget calculations. These deviations are usually located at mountain areas with high-surface albedo, such as the Pamir and Himalaya mountains.

4.3 Implications of the 3-D topography effect on climate modeling

In this study of the 3-D topography effect on clear sky surface solar radiation over the Tibetan Plateau, we find that the entire region receives more solar energy, due primarily to additional reflected fluxes, as shown in Fig. 4a. Additionally, the southern slope of the Himalayas receives more

direct solar fluxes because of a smaller solar incident angle. As a result, if the topography effect is taken into consideration, more sensible and latent heat could be transferred from the surface to the atmosphere, and a stronger Indian monsoon could be produced by climate models. Furthermore, the time of monsoon onset could also be shifted earlier.

Flux deviations as a result of the shading effect could also trigger more convection. For example, the sun-facing sides of mountains receive more solar energy. Air parcels near the mountain surface are heated more than those on a flat surface and will have a tendency to reach the level of free convection. There will therefore be more convection events, and convection could happen earlier than predicted by conventional weather or climate models. Furthermore, the heating difference in the sunward and shaded sides of mountains could produce more small-scale circulations.

Large positive flux deviations are found at high-albedo snow-covered areas, primarily due to direct-reflected- and coupled fluxes. Consequently, these areas would receive much more solar energy than what is estimated by conventional plane-parallel radiative transfer schemes. For this reason, current climate models may be substantially underestimating the rate of snowmelt.

5 Conclusions

To calculate clear sky surface solar fluxes over irregular and intense topography, an improved parameterization approach based on the results simulated from the 3-D Monte Carlo photon tracing program is used to determine flux differences between 1-D unobstructed horizontal and 3-D mountainous surfaces by using the elevation data at a 90-m resolution. The surface solar flux is classified into five components, based on which the relative deviations of these flux components over mountains from the plane-parallel counterpart are expressed in terms of linear combinations of topographic information, including the elevation, slope, solar incident angle, sky view factor, and terrain configuration factor.

We show that over the Tibetan Plateau on 21 March 2001 (spring equinox), the largest deviations in the direct flux with reference to plane-parallel results are about −200 and 200 W/m^2 on the shaded and sunward sides of the mountains, respectively. Over high-albedo snow-covered areas, the largest deviations in the direct-reflected- and coupled fluxes are about 200 and 40 W/m^2, respectively. Combining all five components, deviations in the net surface solar flux range from −150 to 180 W/m^2 over the Tibetan Plateau. The local deviation in the solar flux could lead to earlier onset of convection and more small-scale circulation. The domain-averaged deviations in surface solar fluxes over the whole Tibetan Plateau is on the order of 14 W/m^2 at noon of spring equinox, in which the dominant term is the direct-reflected flux, while the contribution of other components is almost 0. This shows that the surface receives more solar energy than the results calculated from conventional 1-D models, which could lead to stronger convection and enhanced snowmelt rate. While the deviations discussed above are based on the grid size of 10×10 km^2, significant deviations on the order of 20 W/m^2 can be found even at a resolution of 100×100 km^2.

Finally, while the current parameterization approach has been developed for clear sky surface solar flux, it should be noted that because the direct- and direct-reflected fluxes do not encounter atmospheric multiple scattering, the regression equations for these fluxes remain unchanged in cloudy conditions. As a first approximation, the coefficients obtained for clear sky conditions can be applied directly to cloudy conditions. In mountainous areas, however, cloud issues are more complex and require further research and analysis.

Acknowledgments The research work presented in this paper was supported by the National Science Council, Taiwan under contracts NSC101-2111-M-001-001, NSC100-2119-M-001-029-MY5, and NSC98-2111-M-034-004-MY3, Academia Sinica, DOE Grant DE-SC0006742, and NSF Grant AGS-0946315.

References

Chen Y, Hall A, Liou KN (2006) Application of 3D solar radiative transfer to mountains. J Geophys Res 111:D21111. doi:10.1029/2006JD007163

Dozier J, Frew J (1990) Rapid calculations of terrain parameters for radiation modeling from digital elevation data. IEEE Trans Geosci Remote Sens 28:963–969. doi:10.1109/36.58986

Dubayah R, Rich P (1995) Topographic solar radiation models for GIS. Int J Geogr Inf Sci 9:405–419. doi:10.1080/02693799508902046

Dubayah R, Dozier J, Davis FW (1989) The distribution of clear-sky radiation over varying terrain. Proceedings IGARSS '89 vol. 2: 885–888, IEEE 89CH2768-0

Dubayah R, Dozier J, Davis FW (1990) Topographic distribution of clear-sky radiation over the Konza Prairie, Kansas. Water Resour Res 26:679–690. doi:10.1029/89WR03107

Essery R, Marks D (2007) Scaling and parameterization of clear-sky solar radiation over complex topography. J Geophys Res 112: D10122. doi:10.1029/2006JD007650

Fu Q, Liou KN (1992) On the correlated *k*-distribution method for radiative transfer in nonhomogeneous atmospheres. J Atmos Sci 49:2139–2156. doi:10.1175/1520-0469(1992) 049<2139:OTCDMF>2.0.CO;2

Govaerts YM, Verstraete MM (1998) Raytran: a Monte Carlo ray tracing model to compute light scattering in three-dimensional heterogeneous media. IEEE Trans Geosci Remote Sens 36:493–505

Gu Y, Farrara J, Liou KN, Mechoso CR (2003) Parameterization of cloud-radiation processes in the UCLA general circulation model. J Climate 16:3357–3370. doi:10.1175/1520-0442(2003) 016<3357:POCPIT>2.0.CO;2

Gu Y, Liou KN, Xue Y, Mechoso CR, Li W, Luo Y (2006) Climatic effects of different aerosol types in China simulated by the UCLA atmospheric general circulation model. J Geophys Res 111: D15201. doi:10.1029/2005JD006312

Iwabuchi H, Kobayashi H (2008) Modeling of radiative transfer in cloudy atmospheres and plant canopies using Monte Carlo methods. FRCGC Technical Report 8: pp 199

Jarvis A, Reuter HI, Nelson A, Guevara E (2008) Hole-filled seamless SRTM data V4, International Centre for Tropical Agriculture (CIAT), available from http://srtm.csi.cgiar.org

Lai Y-J, Chou M-D, Lin P-H (2010) Parameterization of topographic effect on surface solar radiation. J Geophys Res 115:D01104. doi:10.1029/2009JD012305

Lee W-L, Liou KN (2007) A coupled atmosphere–ocean radiative transfer system using the analytic four-stream approximation. J Atmos Sci 64:3681–3694

Lee W-L, Liou KN, Hall A (2011) Parameterization of solar fluxes over mountain surfaces for application to climate models. J Geophys Res 116:D01101. doi:10.1029/2010JD014722

Liou KN, Lee W-L, Hall A (2007) Radiative transfer in mountains: application to the Tibetan Plateau. Geophys Res Lett 34:L23809. doi:10.1029/2007GL031762

Mayer B, Hoch SW, Whiteman CD (2010) Validating the MYSTIC three-dimensional radiative transfer model with observations from the complex topography of Arizona's Meteor Crater. Atmos Chem Phys 10:8685–8696

Molnar P, England P, Martinod J (1993) Mantle dynamics, uplift of the Tibetan Plateau, and the Indian monsoon. Rev Geophys 31:357–396

Preseindorfer RW, Mobley CD (1986) Albedos and glitter patterns of a wind-roughened sea surface. J Phys Oceanogr 16 (7):1293–1316

Qiu J (2008) China: the third pole. Nature 454:393–396

Wang Q, Tenhunen J, Schmidt M, Otieno D, Kolcun O, Droesler M (2005) Diffuse PAR irradiance under clear skies in complex alpine terrain. Agric For Meteorol 128:1–15. doi:10.1016/j.agrformet.2004.09.004

Yang K, Pinker RT, Ma Y et al (2008) Evaluation of satellite estimates of downward shortwave radiation over the Tibetan Plateau. J Geophys Res 113:D17204. doi:10.1029/2007JD009736